Supplement of The Cryosphere, 14, 2469–2493, 2020
https://doi.org/10.5194/tc-14-2469-2020-supplement

The Cryosphere Open Access EGU

Supplement of

Satellite passive microwave sea-ice concentration data set inter-comparison for Arctic summer conditions

Stefan Kern et al.

Correspondence to: Stefan Kern (stefan.kern@uni-hamburg.de)

S1.1 Comparison to ship-based visual sea-ice observations: Data & Methodology

For our inter-comparison of the 10 products, we also used ship-based manual visual observations of the summer-time sea-ice conditions collected under the IceWatch/ASSIST (Arctic Ship-based Sea-Ice Standardization, see http://icewatch.gina.alaska.edu or https://icewatch.met.no/). Such observations, carried out hourly from the ships' bridge while the ship navigates through the sea ice, provide information about, e.g., total and partial sea-ice concentrations, status of the ice surface and melt-pond concentration. We refer to Worby et al. (2008) and Hutchings and Orlich (2019) for more details. Ship-based observations of the ice conditions have been used already in the past to evaluate PMW SIC products in the otherwise data sparse Arctic region (e.g., Alekseeva et al., 2019; Kern et al., 2019; Wang et al., 2018; Xie et al., 2013; Spreen et al., 2008). We use observations provided in a standardized format from https://doi.org/10.26050/WDCC/ESACCIPSMVSBSIO, last access date: 28 October, 2019. Standardization means that the resulting ascii format data file containing all observations uses similar formats for all variables and missing data. The data are also manually quality checked for outliers. We use all observations during months May through September, for the period June 2002 through December 2011. Figure S01 illustrates the location of the ship tracks from which we used such observations, colour coded with respect to the year of observation. Note that while observations of the sea-ice concentration were made throughout all these tracks, observations of melt ponds are sparser and only available for about one third of the locations shown in Fig. S01.

We co-locate the sea-ice concentrations of the 10 products with the selected ship-based observations by computing the minimum distance between geographic location of the ship-based observation and the grid cell centre of the respective sea-ice concentration product at its native resolution. For this step, we convert the geographic coordinates of all data sets into Cartesian coordinates taking into account the different projections of the sea-ice concentration products. After co-location, we compute daily along-track averages of the ship- and satellite-based sea-ice concentrations following the approach of Beitsch et al. (2015). We discard data pairs with less than three observations per day.

S2.1 Comparison to ship-based visual sea-ice observations: Results

This study so far considered only one source of non-PMW SIC and ISF, namely the dataset of Rösel et al., (2011; 2012a) based on MODIS data. In this section, we report on an alternative source of SIC and ISF information, and assess if comparisons with the new data consolidate our conclusions. Kern et al. (2019) carried out an inter-comparison between the 10 products used here and manual visual ship-based observations of the sea-ice cover. Here we extend this analysis by showing a similar comparison focussing on summer (May through September) of years 2002-2011 (see Sect. S1.1 in the supplementary material) in Fig. S02. We use ship-based observations of the sea-ice concentration as well as of the net ice-surface fraction. We refer to Kern et al. (2019) for a discussion of the quality and limitations of such observations and note here that our main intention for showing this inter-comparison is to confirm the different results of the inter-comparison between PMW SIC and MODIS SIC (Sect. 4.1) or MODIS ISF (Sect. 4.2). Figure S02 suggests agreement between PMW SIC and the ship-based SIC observations which is different for groups II and IV (Fig. S02e-g, j) than for groups I (Fig. S02a-d) and III (Fig. S02h, i) – similar to our results in Sects. 4.1 and 4.2. Overall, SIC differences are smaller for groups II and IV than the other two groups while the standard deviation of the differences is smallest for group I products. For group II and IV products, we find that high PMW SIC larger than 95 % is associated with a considerably larger range of ship-based SIC observations in the scatterplots shown. Nevertheless, the statistical parameters suggest that CBT-SSMI and NOAA CDR of group II agree well with the ship-based SIC observations while group III products are biased low by between ~ -5 % (ASI-SSMI) and ~ -12 % (NT1-SSMI) and the SICCI/OSISAF products (group I) by ~ -9 %. These differences are in line with the results of the comparison between PMW SIC and MODIS SIC (see e.g. Fig. 6) in the sense that group II products provide the highest PMW SIC, group III the lowest and groups I and IV intermediate SIC values.

The value pairs of PMW SIC and ship-based ISF (red dots) also confirm our observations from Sect. 4.2. For group I and ASI-SSMI of group III (Fig. S02a-d, h), the majority of these value pairs fall into the intervals: 75 % ≤ PMW SIC ≤ 100 % and 50 % ≤ ship-based ISF ≤ 75 %, corresponding to an average over-estimation of the ISF by ~25 %. We note that for NT1-SSMI (Fig. S02i), the value pairs are less clustered and closer to the identity line than for any other product, suggesting a smaller difference between PMW SIC and ship-based ISF. For groups II and IV (Fig. S02e-g, j), most PMW SIC values cluster close to 100%; accordingly, the majority of these values pairs fall into the intervals: 90 % ≤ PMW SIC ≤ 100 % and 50 % ≤ ship-based ISF ≤ 75 %, suggesting an average over-estimation of the ISF by ~35 %. This order of the magnitude by which the ship-based ISF is over-estimated by the PMW SIC of the different groups is in line with our results from Sect. 4.2 as well.

S3.1 Using non-truncated sea-ice concentrations

Our results presented in Sects. 3 and 4 are based on truncated sea-ice concentrations, i.e. SIC values set to exactly 100 % (exactly 0 %) in case the natural retrieval results in values larger than 100 % (less than 0 %); see Kern et al. (2019) for more details. Group I (see Table 1) offers non-truncated SIC values. We repeat our analyses with these non-truncated values and show selected results in Fig. S03 and Table S01. A substantial fraction of the value pairs of the 2-D histograms for the period 2003 to 2011 is located above the horizontal dotted line indicating 100 % PMW SIC – here for group I product OSI-450 (Fig. S03, top row). Particularly during pre-melt (Fig. S03a) and melt advance (Fig. S03b) we find counts close to 1000 for PMW SIC values up to 105 % and 110 %, respectively; these are all set to 100 % in Fig. S03e and f. The number of data points with PMW SIC larger than 100 % is much smaller for peak melt (Fig. S03c). Hence, using non-truncated PMW SIC

values has little impact on the statistical inter-comparison results during peak melt. However, during melt advance the slope between PMW SIC and MODIS SIC and, more importantly, between PMW SIC and MODIS ISF increases – together with a small increase in the linear correlation coefficient (see Table S01). Because of this finding it could have been an advantage to carry out the bias correction described in Sect. 4.3 using the non-truncated instead of the truncated PMW SIC data – especially for the melt advance (see Fig. S11, supplementary material). But at this stage further investigations into this topic are beyond the scope of this paper.

Table S01. Linear correlation and slope of the linear regression between group I OSI-450 sea-ice concentration and MODIS SIC (top part) or MODIS ISF (bottom part) for years 2003-2011 illustrating the difference between using truncated or non-truncated PMW SIC values in the 2-D histograms of the kind shown in Figs. S1 and S3. For pre melt and peak melt only the two 8-day periods directly next to the melt-advance period are shown. Numbers in bold font denote a correlation being larger by 0.02 and a slope being larger by 0.5 because of using non-truncated instead of truncated PMW SIC values.

		Pre-melt		Melt advance					Peak melt	
MODIS SIC	8-day period	137	145	153	161	169	177	185	193	201
Correlation	truncated	0.44	0.49	0.56	0.70	0.66	0.67	0.73	0.82	0.86
	non-truncated	0.44	0.48	0.56	0.70	0.67	0.68	0.73	0.82	0.86
Slope	truncated	0.913	1.022	1.117	1.331	1.185	0.935	0.943	1.144	1.269
	non-truncated	0.945	1.045	1.145	**1.407**	**1.294**	**1.001**	0.959	1.154	1.277
MODIS ISF										
Correlation	truncated	0.43	0.48	0.58	0.78	0.78	0.79	0.76	0.82	0.86
	non-truncated	0.41	0.47	0.58	0.78	**0.80**	**0.81**	0.77	0.83	0.86
Slope	truncated	0.467	0.466	0.510	0.679	0.676	0.621	0.670	0.801	0.891
	non-truncated	0.468	0.469	0.519	0.718	**0.743**	**0.678**	0.689	0.810	0.899

S3.2 Additional Supplementary Material

Figure S04 provides maps of the sea-ice concentration difference between all 10 individual products and the ensemble mean sea-ice concentration similar to Fig. 3 where only maps of the four products representative of the four groups are shown.

Figure S05 adds upon Fig. 4 showing the scatterplots between PMW SIC and MODIS SIC for the four groups obtained for the entire period 2003-2011. The same applies to Fig. S06 which adds upon Fig. 7, showing scatterplots between PMW SIC and MODIS ISF in the same way.

Figure S06 complements Fig. 4 and Fig. S05 in that is shows the respective scatterplots between PMW SIC and MODIS SIC for the pre-melt case. Figure S09 complements Fig. 7 and Fig. S08 in the same way but showing MODIS ISF instead of MODIS SIC.

Figures S07 and S10 complement Figs. 6 and 9 by showing respective parameters for all 10 products instead of just the four representative ones.

Figure S11 finally shows the results of the bias-correction of PMW SIC based our findings from the comparison between MODIS ISF and PMW SIC for a melt-advance case, complementing the peak-melt case shown in Fig. 10.

S4. References

Alekseeva, T. Tikhonov, V., Frolov, S., Repina, I., Raev, M., Sokolova, J., Sharkov, E., Afanasieva, E., and Serovetnikov, S.: Comparison of Arctic sea ice concentration from the NASA Team, ASI, and VASIA2 algorithms with summer and winter ship data, Rem. Sens., 11(21), 2481, http://doi.org/10.3390/rs11212481, 2019.

Beitsch, A., Kern, S., and Kaleschke, L.: Comparison of SSM/I and AMSR-E sea ice concentrations with ASPeCt ship observations around Antarctica, IEEE Trans. Geosci. Rem. Sens., 53(4), 1985-1996, http://doi.org/10.1109/TGRS.2014.2351497, 2015.

Hutchings, J. K., and Orlich, A. R.: A standardized protocol and database for discrete visual observations of Arctic sea ice. Earth System Sci. Data, submitted, 2018.

Kern, S., Lavergne, T., Notz, D., Pedersen, L., Tonboe, R., Saldo, R., and Sørensen, A. M.: Satellite Passive Microwave Sea-Ice Concentration Data Set Intercomparison: Closed Ice and Ship-Based Observations, The Cryosphere, 13(12), 3261-3307, http://doi.org/10.5194/tc-13-3261-2019, 2019.

Rösel, A., and Kaleschke, L.: Comparison of different retrieval techniques for melt ponds on Arctic sea ice from Landsat and MODIS satellite data. Ann. Glaciol., 52, 185–191, 2011.

Rösel, A., Kaleschke, L., and Birnbaum, G.: Melt ponds on Arctic sea ice determined from MODIS satellite data using an artificial neural network. The Cryosphere, 6, 431-446, http://doi.org/10.5194/tc-6-431-2012, 2012a.

Spreen, G., Kaleschke, L., and G. Heygster, G.: Sea ice remote sensing using AMSR-E 89-GHz channels, J. Geophys. Res., 113, C02S03, http://doi.org/10.1029/2005JC003384, 2008.
Wang, Q., Li, Z., Lu, P., Lei, R., and Cheng, B.: 2014 summer Arctic sea ice thickness and concentration from shipborne observations. Int. J. Digi. Earth, Jan. 5 2018, http://doi.org/10.1080/17538947.2017.142.1720, 2018.
Worby, A. P., Geiger, C. A., Paget, M. J., Van Woert, M. L., Ackley, S. F., and DeLiberty, T. L.: The thickness distribution of Antarctic sea ice. J. Geophys. Res., 113, C05S92, http://doi.org/10.1029/2007JC004254, 2008.
Xie, H., Lei, R., Ke, C., Wang, H., Li, Z., Zhao, J., and Ackley, S. F.: Summer sea ice characteristics and morphology in the Pacific Arctic sector as observed during the CHINARE 2010 cruise. The Cryosphere, 7(4), 1057-1072, http://doi.org/10.5194/tc-7-1057-2013, 2013.

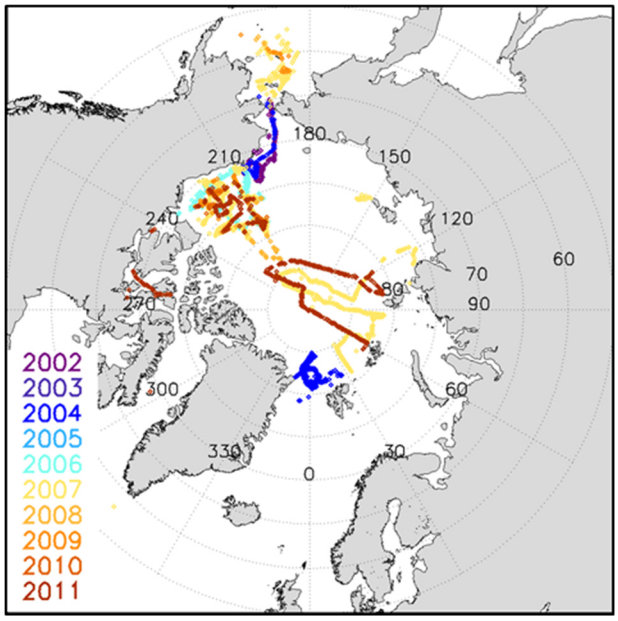

Figure S01. Spatiotemporal distribution of ship tracks in the Arctic from which ship-based visual observations of the sea-ice cover were used.

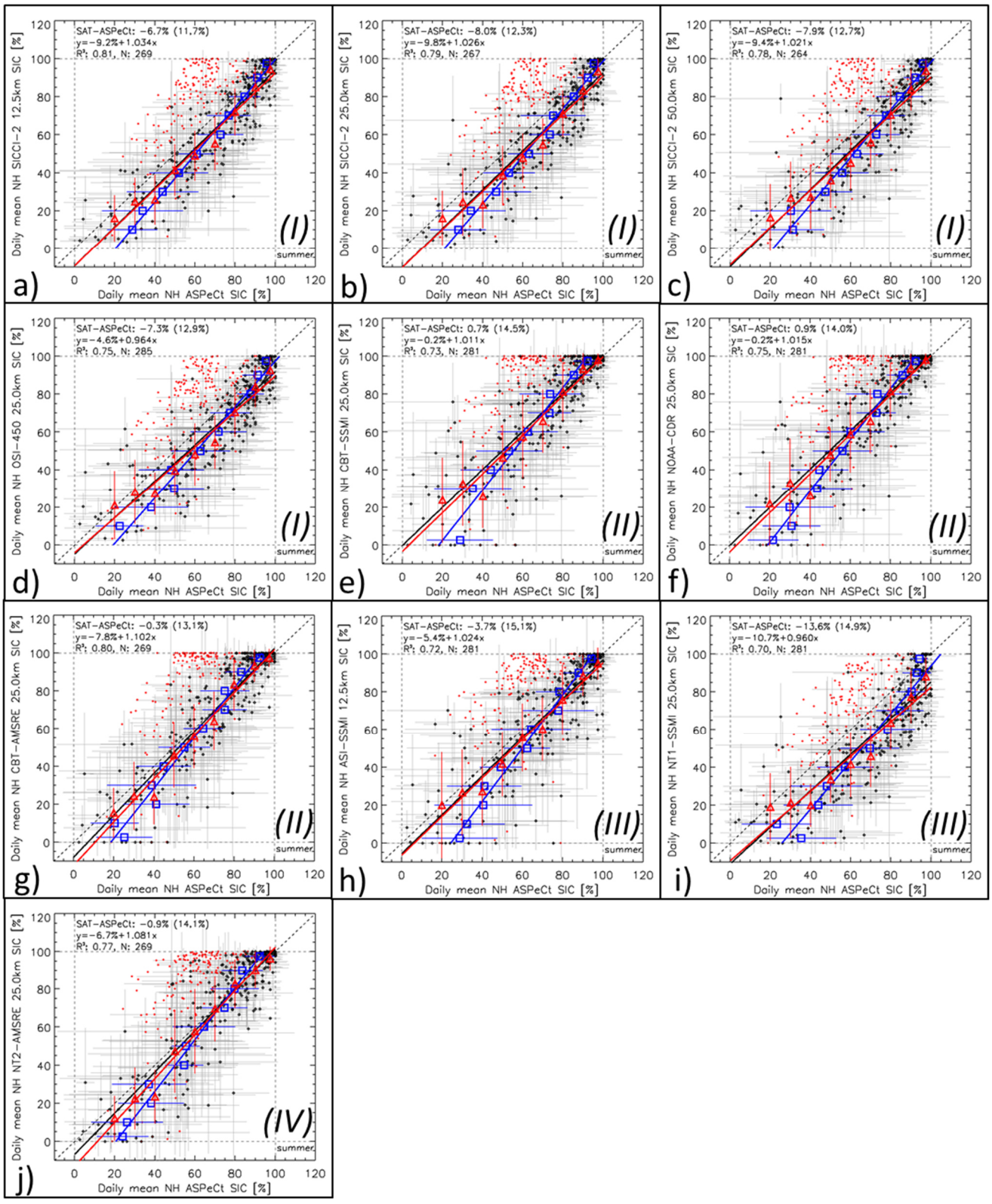

Figure S02. Scatterplots of co-located daily average SIC (black dots) and average ice-surface fraction (red dots) from visual ship-based observations (ASPeCt, x-axis) and the ten satellite SIC algorithm products (SAT, y-axes) for the Arctic for May through September for years 2002-2011 (see Fig. S01 for locations). Error bars denote one standard deviation of the average. Dotted lines denote the identity line. Solid lines denote the linear regression of the SIC data pairs. The mean difference (standard deviation), the linear regression equation, the squared linear correlation coefficient (R^2) and the number of valid data pairs N is given in the top left of every image for the daily SIC value data pairs. Red triangles (blue squares) denote the average SAT SIC at 10 % wide ship-based SIC bins (average ship-based SIC at 10 % wide SAT SIC bins). Roman numbers in bold font denote the group (see Table 1) to which the algorithm is assigned.

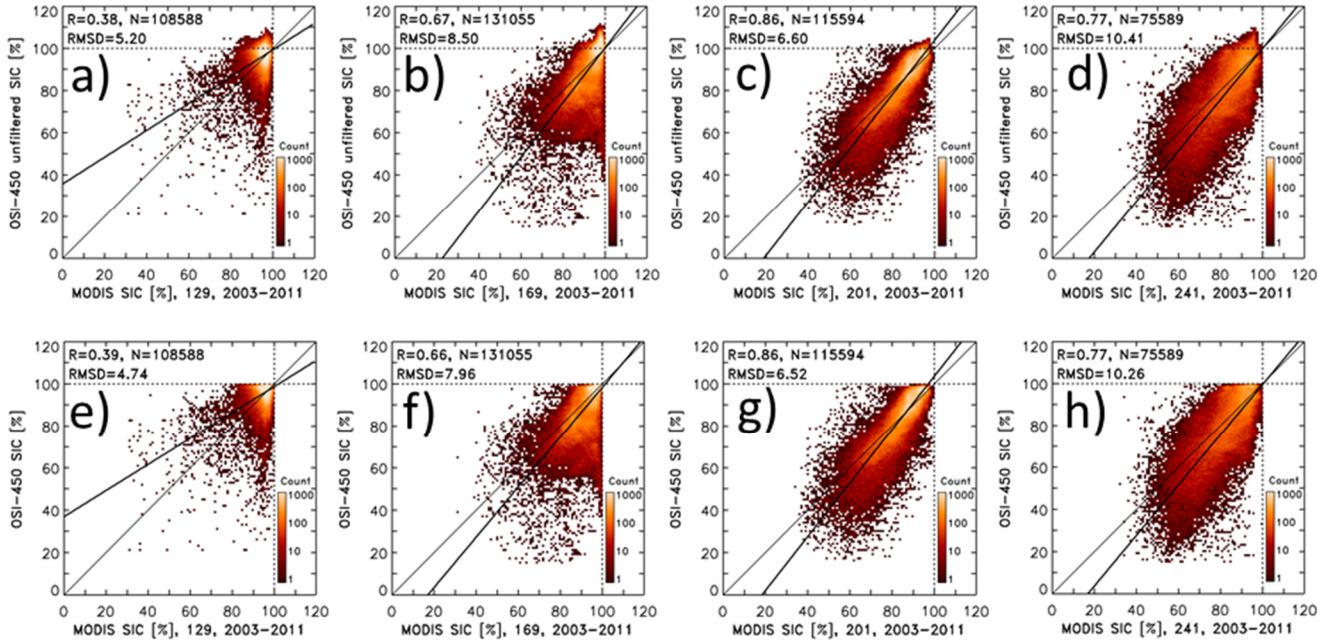

Figure S03. Illustration of the impact using the non-truncated (top row, panel a) to d) instead of the truncated (bottom row, panel e) to h) SIC data, for example OSI-450 (representative of group I products), when comparing PMW SIC with MODIS SIC. Shown are the two-dimensional histograms for all four 8-day periods starting at DOY 129, 169, 201, and 241 of the years 2003 through 2011 (see Fig. S05). The quantities given in the top left corner are R: linear correlation coefficient, N: number of valid data pairs, and RMSD: root mean squared difference. The thin black line is the identity line; the thick black line denotes the linear regression through the data pairs.

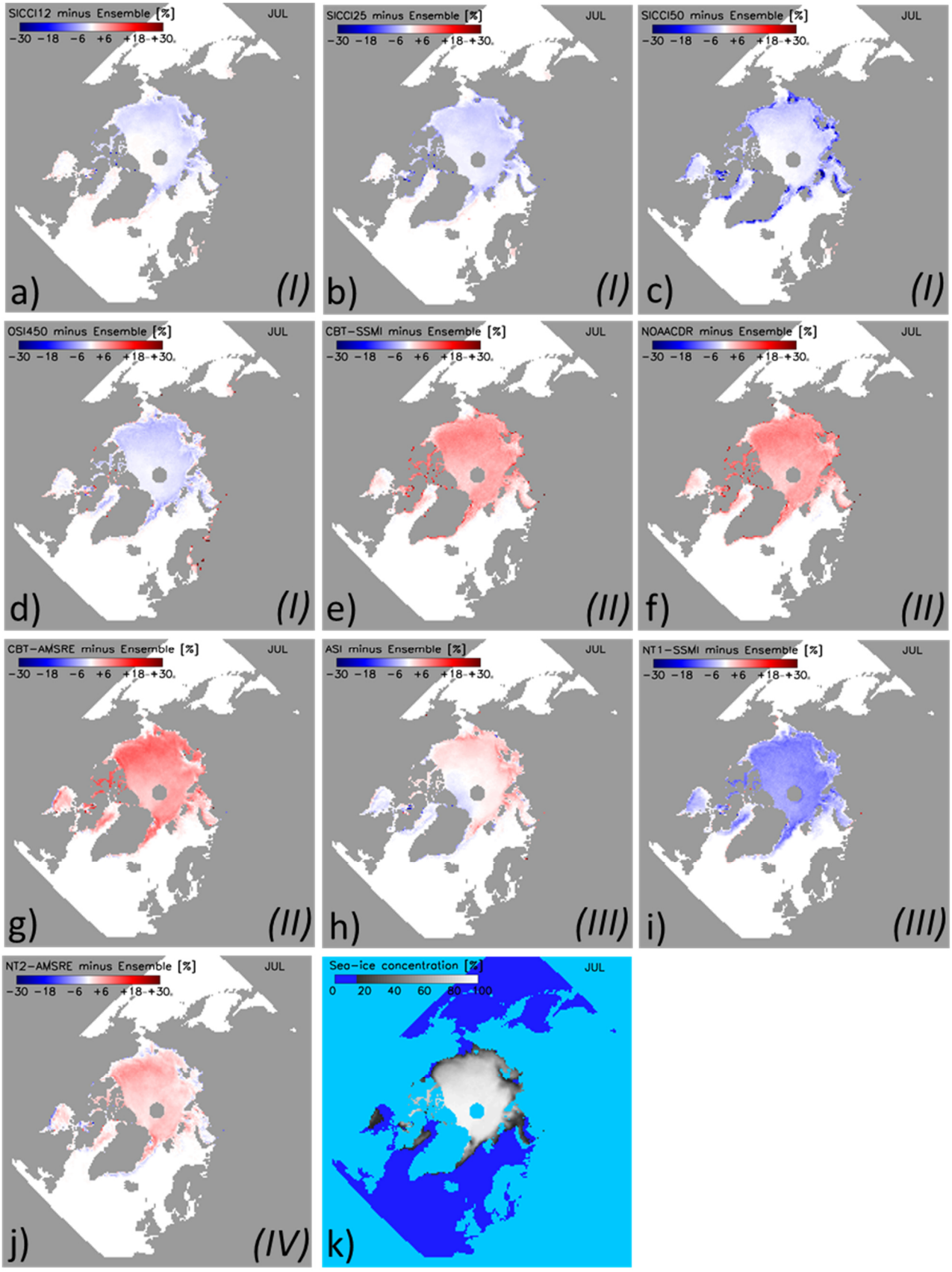

Figure S04. (a) to **(j)** Maps of the difference between the multi-annual average monthly SIC of the individual algorithms and the 10-algorithm ensemble median multi-annual average monthly SIC **(k)** for the Arctic for July 2003-2011 (see also Fig. 3). Differences are only computed for sea-ice concentration of both data sets larger than 15%. Roman numbers in bold font denote the group (see Table 1) to which the algorithm is assigned. We refer to Kern et al. (2019) for an explanation of the large negative differences along some coastlines shown for SICCI-50km (Fig. S04c).

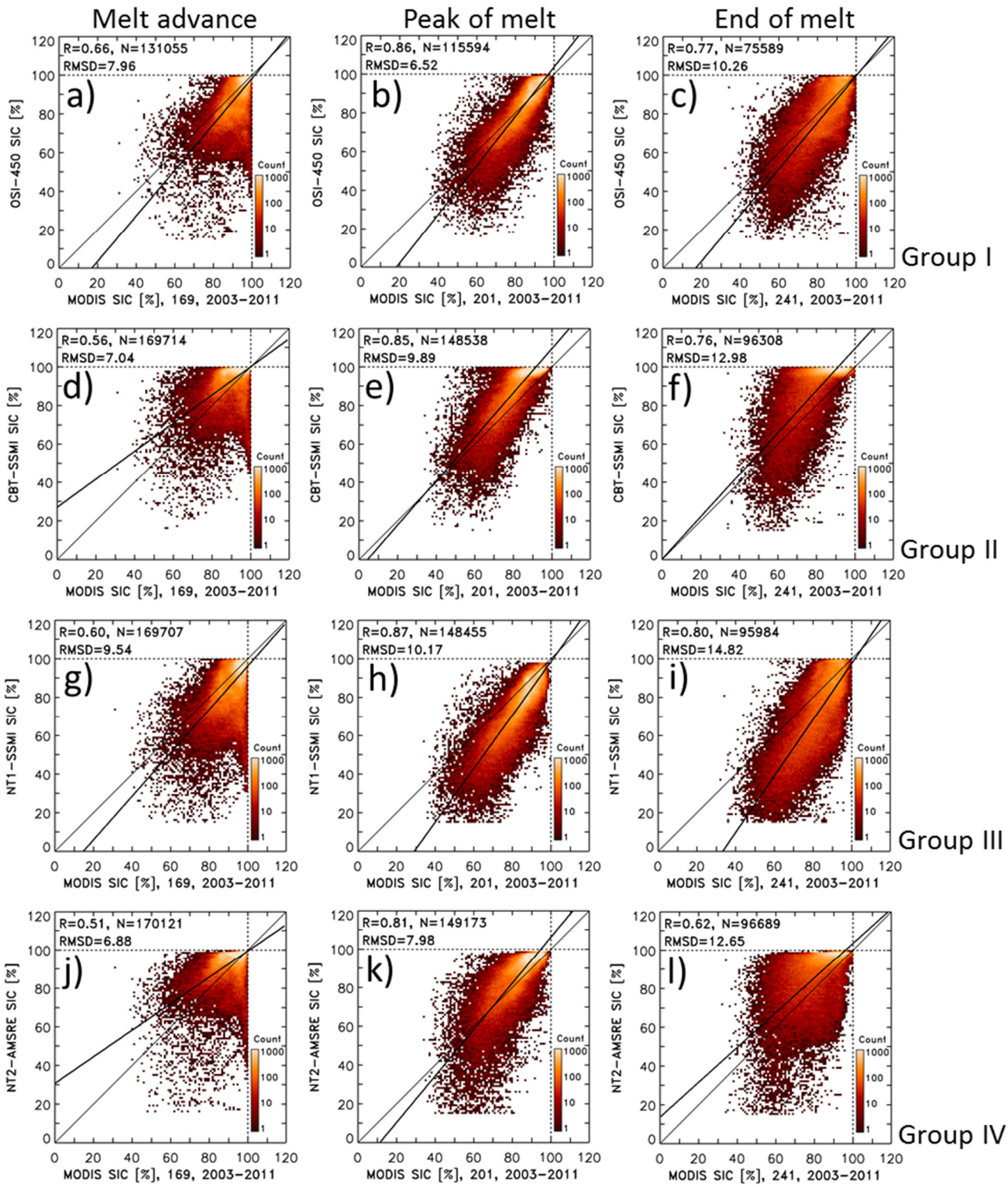

Figure S05. Two-dimensional histograms of the distribution of PMW (y-axis) versus MODIS (x-axis) SIC data pairs using a bin size of 1 % for the same products and 8-day periods as shown in Fig. 4 but for years 2003-2011. The thin black line is the identity line. The thick black line denotes the linear regression through the data pairs. In the top left of every image we display the linear correlation coefficient R, the number of data pairs N and the root mean squared difference RMSD; the latter is given in percent. The leftmost, middle and rightmost columns are representing melt advance, peak of melt, and end of the melt, respectively. Respective scatterplots for pre-melt are shown in Figure S06.

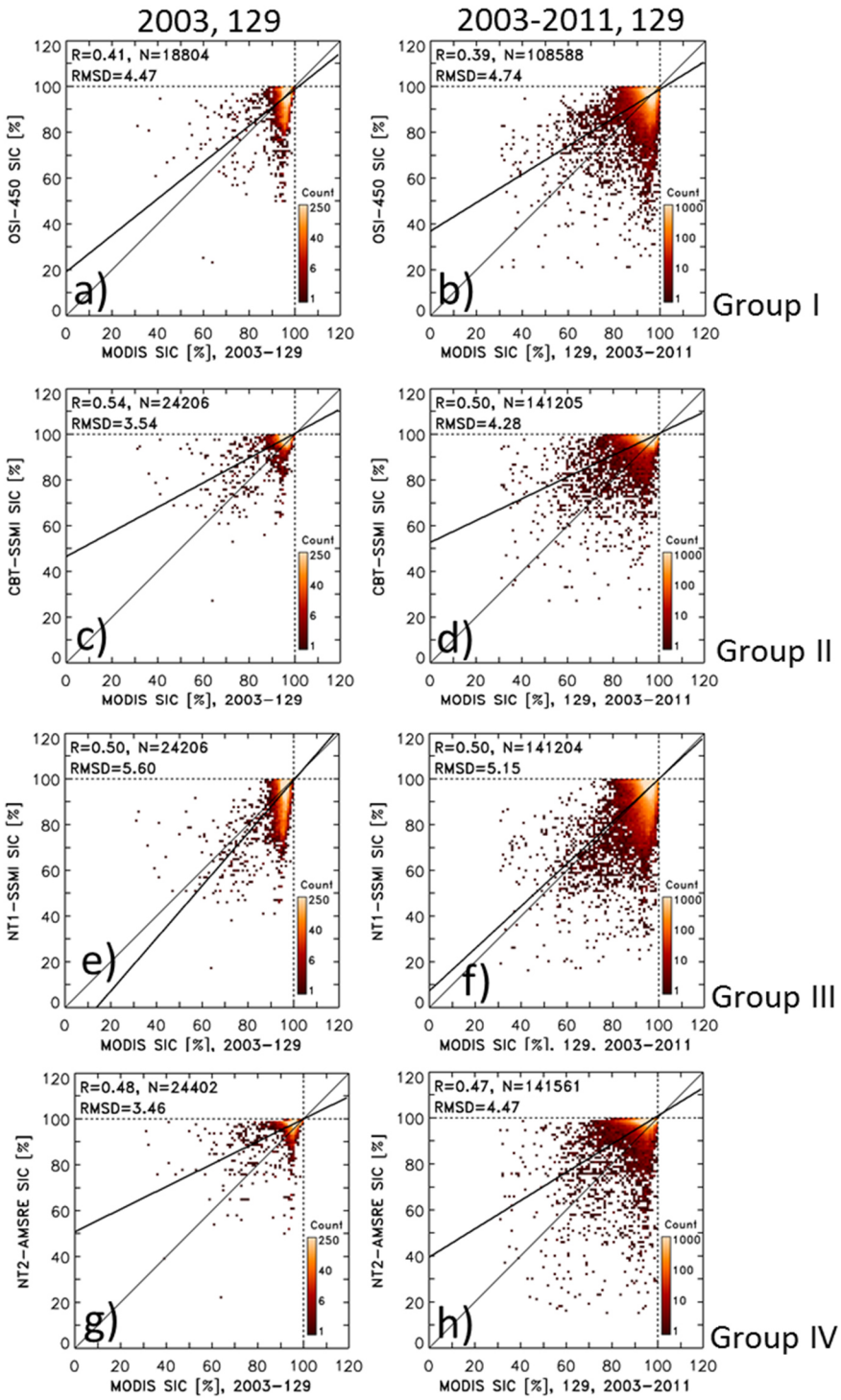

Figure S06. Two-dimensional histograms of the distribution of PMW SIC (y-axis) versus MODIS SIC (x-axis) data pairs using a bin size of 1 % for the same products as shown in Fig. 4 for a pre-melt example, i.e. period DOY 129 (May 9-16) 2003. The left column shows data of a single year (2003), the right column data of years 2003-2011. The topmost row shows OSI-450 (for group I), the second row CBT-SSMI (for group II), the third row NT1-SSMI (for group III), and the bottommost row NT2-AMSRE (group IV). The thin black line is the identity line. The thick black line denotes the linear regression through the data pairs. In the top left of every image we display the linear correlation coefficient R, the number of data pairs N and the root mean squared difference RMSD; the latter is given in percent.

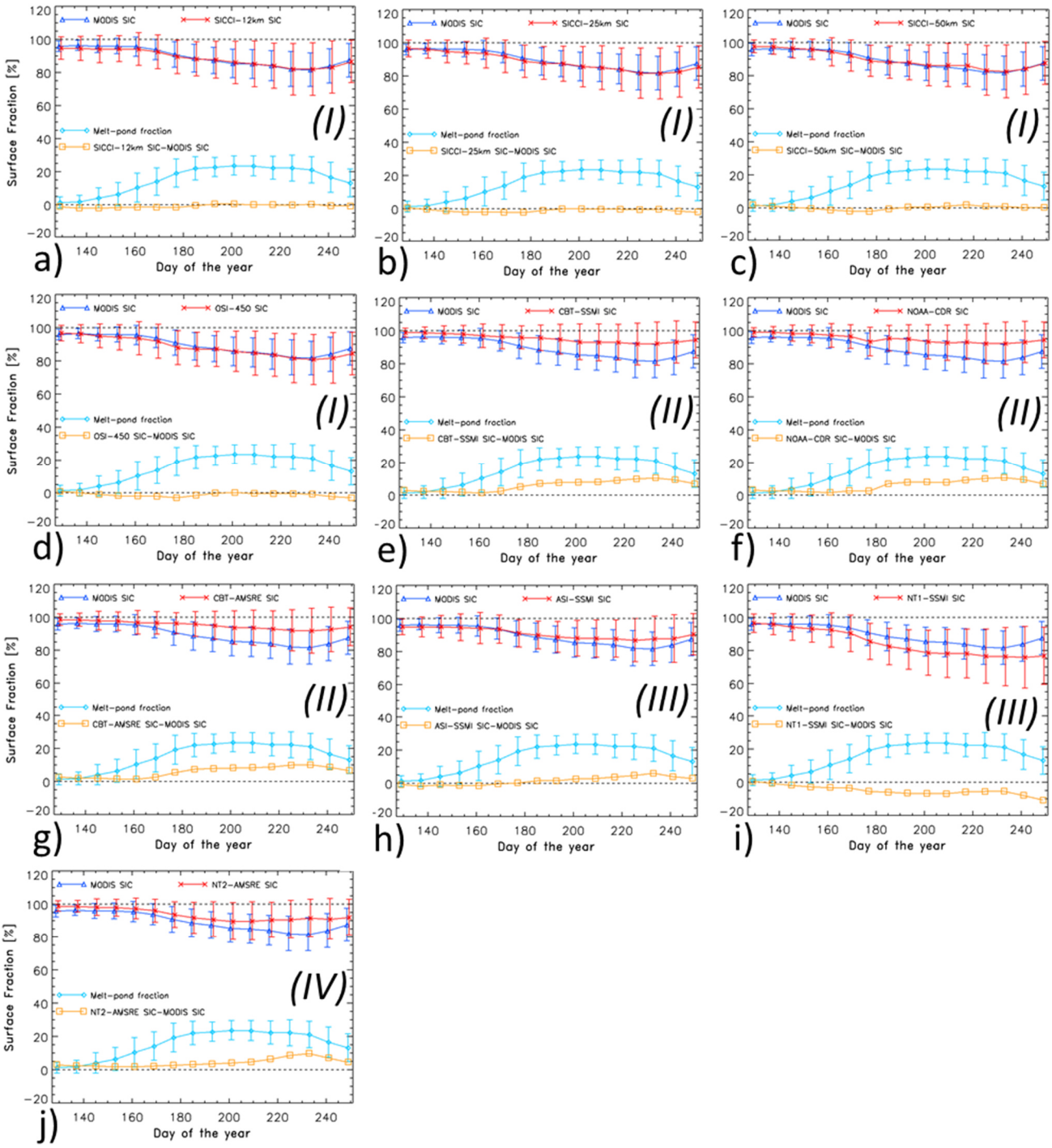

Figure S07. Average seasonal cycle of the mean (limited to Arctic Ocean and Canadian Arctic Archipelago) MODIS SIC (in blue), PMW SIC (in red), their difference PMW minus MODIS SIC (in orange), and the MODIS melt-pond fraction (in cyan), averaged for each 8-day period for the years 2003-2011. Error bars denote one standard deviation of the mean. Roman numbers in bold font denote the group (see Table 1) to which the algorithm is assigned.

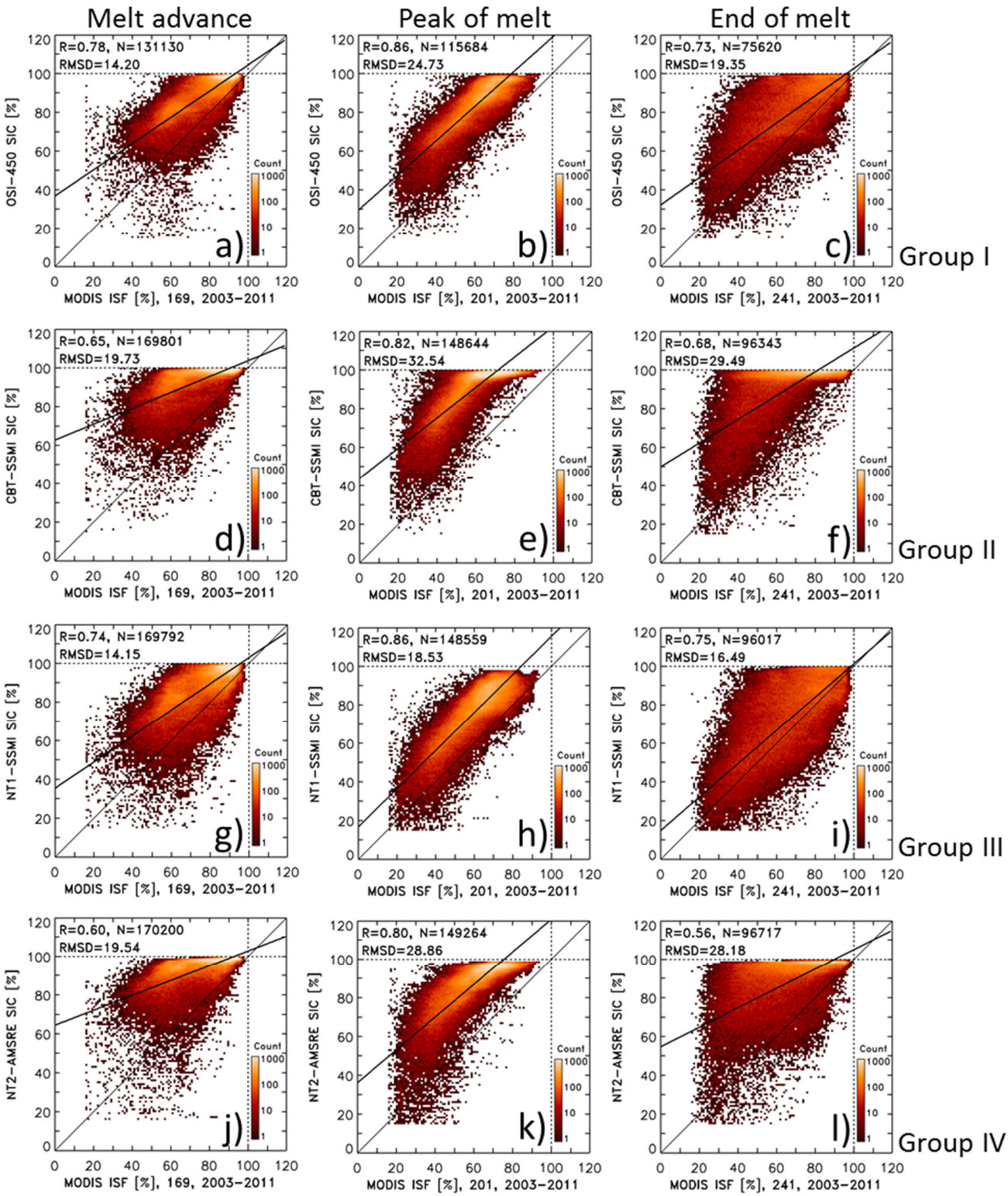

Figure S08. Two-dimensional histograms of the distribution of PMW SIC (y-axis) versus MODIS ISF (x-axis) data pairs using a bin size of 1 % for the same products and 8-day periods as shown in Fig. 7 but for years 2003-2011. The thin black line is the identity line. The thick black line denotes the linear regression through the data pairs. In the top left of every image we display the linear correlation coefficient R, the number of data pairs N and the root mean squared difference RMSD; the latter is given in percent. The leftmost, middle and rightmost columns are representing melt advance, peak of melt, and end of the melt, respectively. Respective scatterplots for pre-melt are shown in Figure S09.

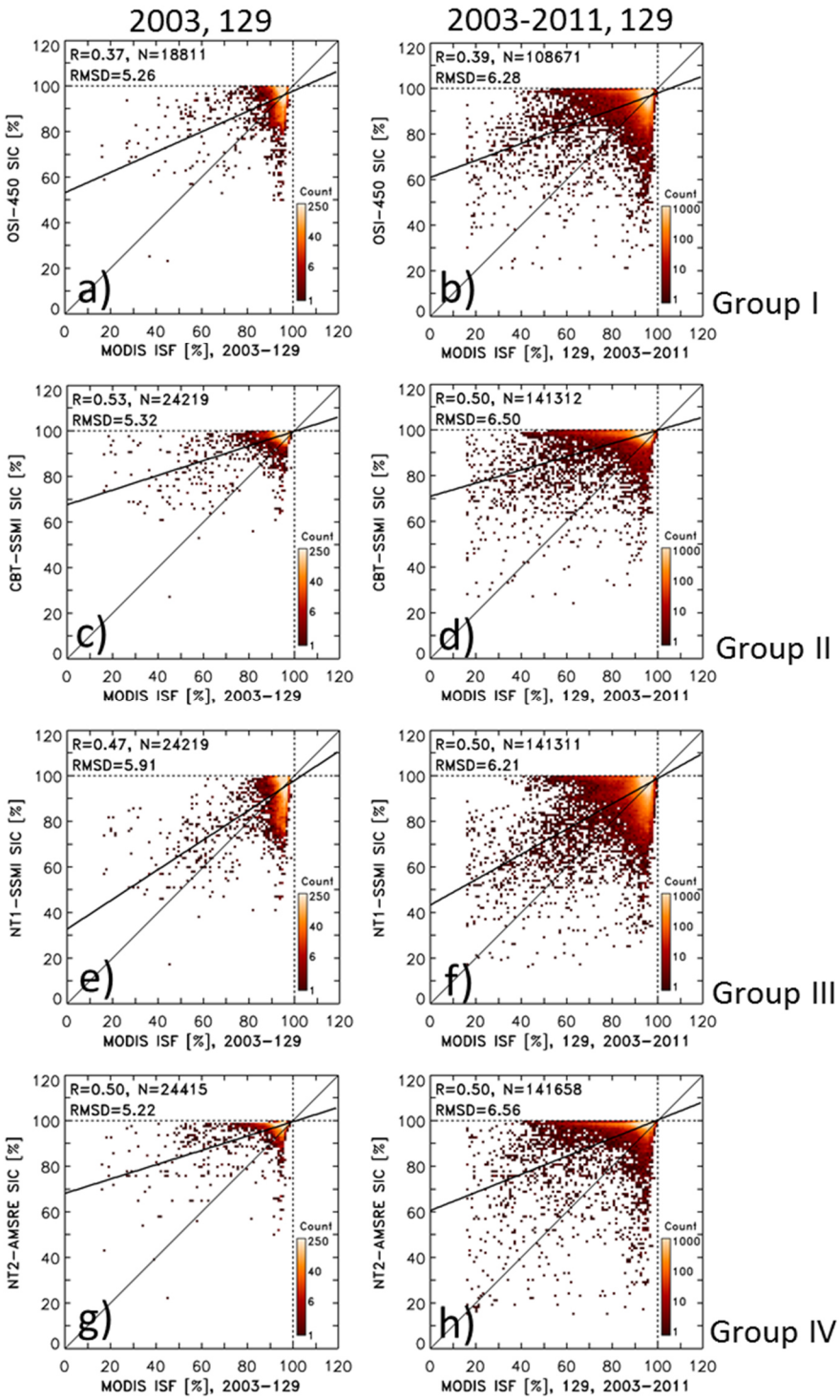

Figure S09. Two-dimensional histograms of the distribution of PMW SIC (y-axis) versus MODIS ISF (x-axis) data pairs using a bin size of 1 % for the same products as shown in Fig. 7 for a pre-melt example, i.e. period DOY 129 (May 9-16) 2003. The left column shows data of a single year (2003), the right column data of years 2003-2011. The topmost row shows OSI-450 (for group I), the second row CBT-SSMI (for group II), the third row NT1-SSMI (for group III), and the bottommost row NT2-AMSRE (group IV). The thin black line is the identity line. The thick black line denotes the linear regression through the data pairs. In the top left of every image we display the linear correlation coefficient R, the number of data pairs N and the root mean squared difference RMSD; the latter is given in percent.

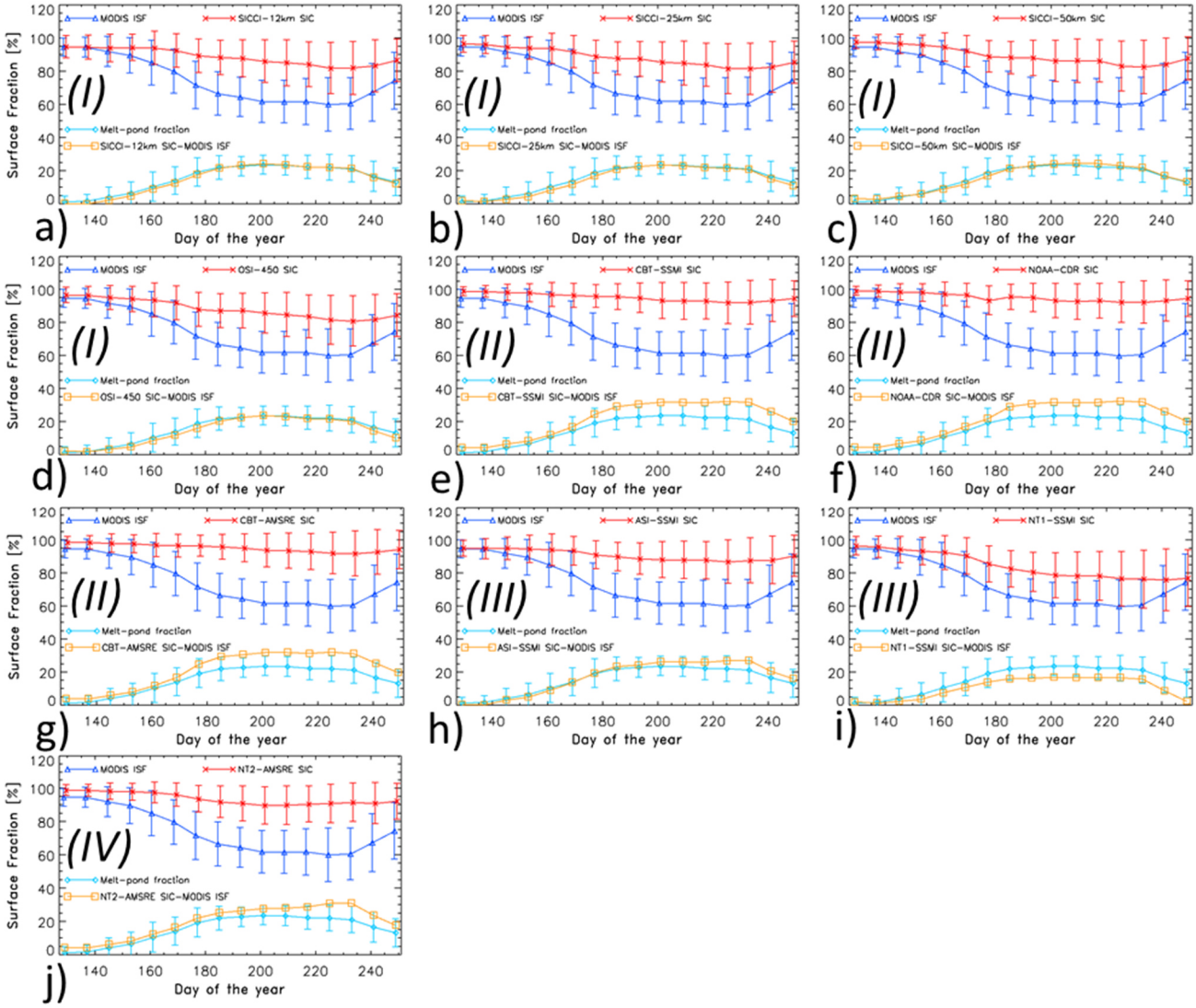

Figure S10. Average seasonal cycle of the mean (limited to Arctic Ocean and Canadian Arctic Archipelago) MODIS ISF (in blue), PMW SIC (in red), their difference PMW SIC minus MODIS ISF (in orange), and the MODIS melt-pond fraction (in cyan), averaged for each 8-day period over the years 2003-2011. Error bars denote one standard deviation of the mean. Roman numbers in bold font denote the group (see Table 1) to which the algorithm is assigned.

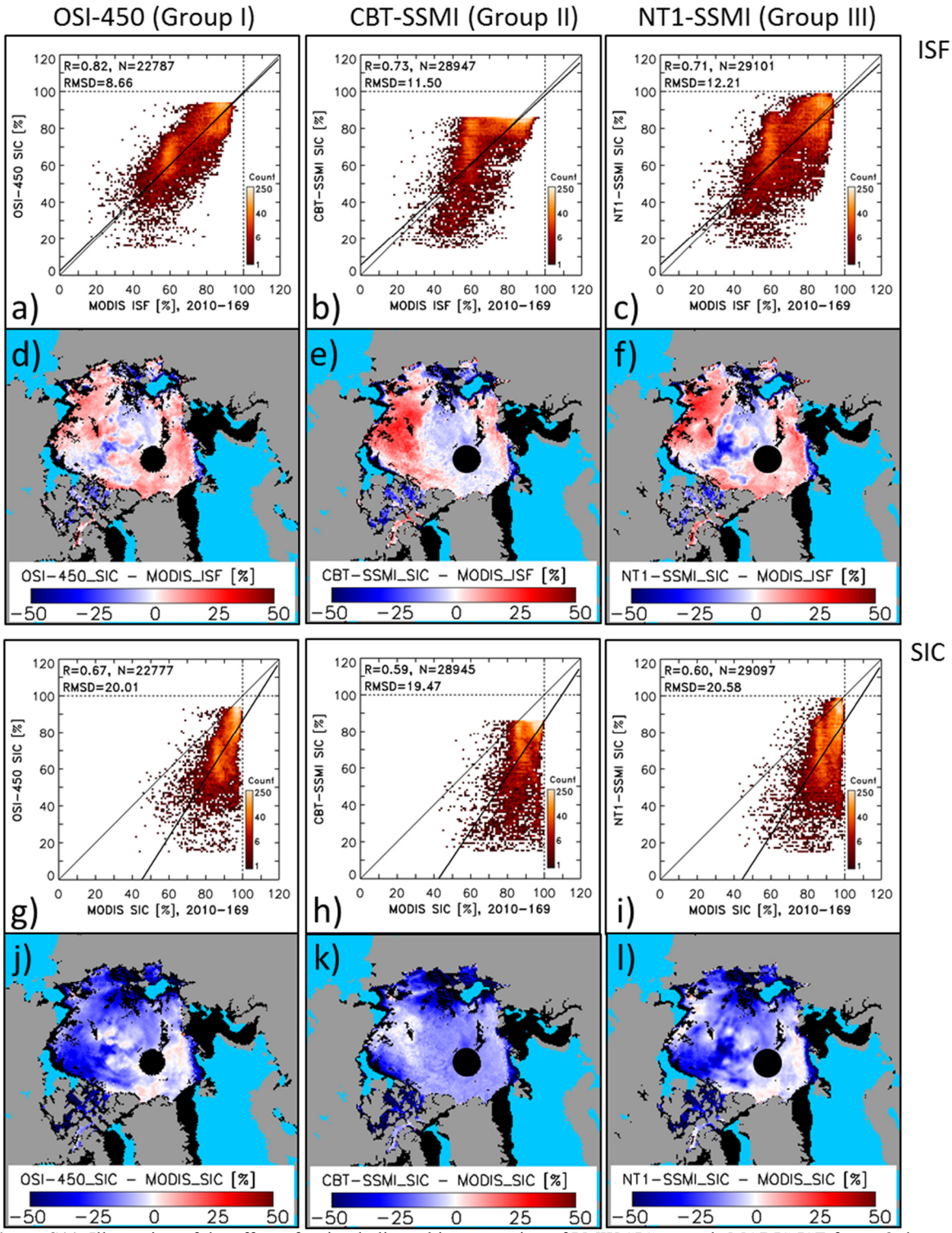

Figure S11. Illustration of the effect of a simple linear bias correction of PMW SIC towards MODIS ISF for an 8-day period during melt advance (DOY 169, June 18-25, 2010). Topmost row, panels a) to c): Two-dimensional histograms of the distribution of bias-corrected PMW SIC (y-axis) versus MODIS ISF (x-axis) data pairs. Second row, panels d) to f): Respective maps of the difference of bias-corrected PMW SIC minus MODIS ISF. Third row, panels g) to i) Two-dimensional histograms of the distribution of bias-corrected PMW SIC (y-axis) versus MODIS SIC (x-axis) data pairs. Bottommost row, panels j) to l): Respective maps of the difference bias-corrected PMW SIC minus MODIS SIC. Leftmost, middle and rightmost columns show OSI-450 (for group I), CBT-SSMI (for group II), and NT1-SSMI (for group III). Bin size in the histograms is 1 %. The quantities given in the top left corner are R: linear correlation coefficient, N: number of valid data pairs, and RMSD: root mean squared difference. The thin black line is the identity line; the thick black line denotes the linear regression through the data pairs.